LA-UR-15-24397 (Accepted Manuscript)

Insights into dynamic processes of cations in pyrochlores and other complex oxides

Uberuaga, Blas P.
Perriot, Romain Thibault

Provided by the author(s) and the Los Alamos National Laboratory (0000-00-00).

To be published in: Physical Chemistry Chemical Physics, 2015.

DOI to publisher's version: 10.1039/c5cp03372a

Permalink to record: http://permalink.lanl.gov/object/view?what=info:lanl-repo/lareport/LA-UR-15-24397

Disclaimer:
Approved for public release. Los Alamos National Laboratory, an affirmative action/equal opportunity employer, is operated by the Los Alamos National Security, LLC for the National Nuclear Security Administration of the U.S. Department of Energy under contract DE-AC52-06NA25396. Los Alamos National Laboratory strongly supports academic freedom and a researcher's right to publish; as an institution, however, the Laboratory does not endorse the viewpoint of a publication or guarantee its technical correctness.

Journal Name

ARTICLE TYPE

Cite this: DOI: 10.1039/xxxxxxxxxx

Insights into dynamic processes of cations in pyrochlores and other complex oxides

Blas Pedro Uberuaga*[a] and Romain Perriot [a]

Received Date
Accepted Date

DOI: 10.1039/xxxxxxxxxx

www.rsc.org/journalname

Complex oxides are critical components of many key technologies, from solid oxide fuel cells and superionics to inert matrix fuels and nuclear waste forms. In many cases, understanding mass transport is important for predicting performance and, thus, extensive effort has been devoted to understanding mass transport in these materials. However, most work has focused on the behavior of oxygen while cation transport has received relatively little attention, even though cation diffusion is responsible for many phenomena, including sintering, radiation damage evolution, and deformation processes. Here, we use accelerated molecular dynamics simulations to examine the kinetics of cation defects in one class of complex oxides, $A_2B_2O_7$ pyrochlore. We find that, in some pyrochlore chemistries, B cation defects are kinetically unstable, transforming to A cation defects and antisites at rates faster than they can diffuse. When this occurs, transport of B cations occurs through defect processes on the A sublattice. Further, these A cation defects, either interstitials or vacancies, can interact with antisite disorder, reordering the material locally, though this process is much more efficient for interstitials than vacancies. Whether this behavior occurs in a given pyrochlore depends on the A and B chemistry. Pyrochlores with a smaller ratio of cation radii exhibit this complex behavior, while those with larger ratios exhibit direct migration of B interstitials. Similar behavior has been reported in other complex oxides such as spinels and perovskites, suggesting that this coupling of transport between the A and B cation sublattices, while not universal, occurs in many complex oxides.

1 Introduction

Complex oxides (defined here as those having more than one cation sublattice) have a multitude of technological applications, from superionics[1] to nuclear energy materials[2,3]. Often, the properties that make the material suitable for a given application are related to the kinetics of defects. This is especially true for radiation damage environments, in which defects are unavoidably created in large numbers. In particular, in contrast to other applications in which relatively mobile and easily manipulated oxygen defects dominate, radiation damage produces defects on the cation sublattices and, as a consequence, cation defect kinetics cannot be ignored. Cation mobility is also key for understanding sintering processes and degradation of oxides during application[4,5].

While most studies of complex oxides focus on anion transport, several studies on cation transport have now revealed that the kinetic processes of cations in complex oxides are rather involved. Whether pyrochlore[6–8], spinel[9,10], or perovskite[11], simulations have shown that cation mobility is not simply governed by the motion of cation vacancies and interstitials through the lattice. Rather, there are complicated interactions between the multiple cation sublattices and species migrate by moving between the two sublattices. In fact, in each material, the migration of one type of cation occurs via the diffusion of defects on the sublattice of the other cation.

Here, we examine in more detail the kinetic processes associated with cation mobility in one complex oxide, pyrochlore. Pyrochlores ($A_2B_2O_7$) are of particular interest to the nuclear energy community as it has been proposed as a potential crystalline waste form for the immobilization of fission products and actinides[2]. Further, pyrochlores are an important class of fast ion

[a] Materials Science and Technology Division, Los Alamos National Laboratory, Los Alamos, NM, USA. E-mail: blas@lanl.gov

Table 1 Short-range parameters for the Buckingham potential used in this study, from Ref. [18]. Formal charges are used for all species (-2 for O, +3 for Lu, and +4 for Ti).

Interaction	A (eV)	ρ (Å)	C (eV/Å^6)
O-O	9547.96	0.2192	32.0
Lu-O	1618.8	0.33849	19.27
Ti-O	2131.04	0.3038	0.0

conductors [12]. There is thus general interest in these materials. In the context of radiation damage, extensive work has examined the properties of these oxides under irradiation, uncovering important correlations between the properties of the material and amorphization susceptibility [13,14]. Even so, there is still much that is not clear regarding the kinetics of cations, processes that are important from the point of view of radiation damage recovery, sintering, and thermal annealing. Our goal is to provide new insight into these properties via computer simulation.

2 Methodology

We use temperature accelerated dynamics (TAD) [15], one of the accelerated molecular dynamics (AMD) methods [16], to simulate the dynamics associated with cation defects in $Lu_2Ti_2O_7$. This composition was chosen as accurate potentials, of the Buckingham form [17], exist for this material. In particular, we use the parameterization by Minervini et al. [18], which is summarized in Table 1. Further, we chose a B=Ti composition because these exhibit strong ordering of the oxygen sublattice, which aids in the use of the TAD method. In contrast, in B=Zr pyrochlores, the structural vacancies on the oxygen sublattice are able to diffuse [19], complicating the identification and characterization of transitions on the cation sublattices.

In the TAD method, a high temperature trajectory is used to explore the current state of the system. As events occur at this high temperature, they are identified and characterized using the nudged elastic band (NEB) method [20]. The trajectory is then placed back into the current state to continue exploring. However, the time at which the event occurred, given knowledge of the saddle point energy (found using NEB), is extrapolated to the low temperature of interest. Once enough time is accumulated at the high temperature, a time that is well defined given a user supplied lower bound on all prefactors ν_{min} and an uncertainty δ, the high temperature trajectory can be stopped, the event with the shortest time at the low temperature accepted, the system placed in the corresponding state, and the procedure repeated. In this way, accurate state-to-state dynamics can be generated for the system, provided harmonic transition state theory holds (a requirement for the extrapolation of times to be accurate).

We note that, in our initial simulation, we had an incorrect value for the C parameter for the Lu-O interaction. However, after reconverging all of the pathways reported in this paper with the correct parameter, most energies changed by less than 0.1 eV and no energies changed by more than 0.3 eV. The only energies that changed to this extent involved the vacancy migration reported in Figure 5, for which all of the associated energetics are much higher in value.

In the simulation described here, the high temperature was set to 5000 K and the low temperature was 3000 K. ν_{min} was 10^{12}/s and δ=0.05. A total time of 0.161 μs was simulated, resulting in a computational speed-up over conventional molecular dynamics of about 1.6 times. This is not an extraordinary speed-up, a consequence of the relatively high low temperature used. However, as a consequence of the TAD algorithm, a great deal of information about the events that occurred is generated, providing detailed insight into the mechanisms responsible for the dynamics. Thus, the goal here was not to generate a long-time trajectory, but to uncover the mechanisms and associated barriers responsible for the cation dynamics. Finally, the simulation temperatures are clearly unphysical. The use of such high temperatures is simply to further accelerate the simulation. However, the energetics we report are from the zero-temperature potential energy surface. Thus, they should be relevant for all temperatures. That said, as discussed below, as there are multiple events competing at any given time, predicting which events would dominate as a function of temperature would require more extensive characterization than we have attempted here.

The system simulated consisted of a $2 \times 2 \times 2$ block of pyrochlore, at the 0K lattice constant, leading to a system with 704 atoms and cell dimensions of 1.998 nm on each side. One Ti interstitial and a cation antisite pair (Lu_{Ti}+Ti_{Lu} as nearest neighbors) were introduced at the beginning of the simulation. In order to observe the dynamics of the defect as it approached the antisite pair, the interstitial was placed at a large distance ($\sim$ 11 Å) from the antisite pair. The simulation was advanced until 3,828 events were accepted, at which point it was determined that no new behavior would be observed. During the course of the simulation, a total of 5,476 unique events were observed and characterized, not all of which were accepted. The behavior of the Ti vacancy was also investigated, in a simulation cell containing a vacancy far ($\sim$ 11 Å) from the antisite pair. The same TAD parameters as for the interstitial case were used for the vacancy case.

The different defects encountered in this study are listed in table 2, along with their Kröger-Vink notation [21] and net charge. In the rest of this paper, we used a simplified notation, as indicated, in which the charges are not explicitly given for simplicity.

Other chemistries were considered to evaluate the generality of the results observed for $Lu_2Ti_2O_7$ (see Sec.3.3). For these, we used a set of Buckingham parameters consistent with those listed in table 1, from Refs [18,22,23].

Finally, density functional theory (DFT) calculations were per-

This journal is © The Royal Society of Chemistry [year]

Table 2 List of defects discussed in the text, with the corresponding Kröger-Vink notation and simplified notation used in the text for $Lu_2Ti_2O_7$, the generic notation used in the text for pyrochlores more generally, and the net charge of the defect.

Defect	Kröger-Vink notation	Simplified notation	Generic notation	Net charge
Ti antisite	$Ti^{\bullet}_{Lu}$	Ti_{Lu}	B_A	+1
Lu antisite	Lu'_{Ti}	Lu_{Ti}	A_B	-1
Ti vacancy	V''''_{Ti}	V_{Ti}	V_B	-4
Lu vacancy	V'''_{Lu}	V_{Lu}	V_A	-3
Ti interstitial	$Ti_i^{\bullet\bullet\bullet\bullet}$	Ti_i	B_i	+4
Lu interstitial	$Lu_i^{\bullet\bullet\bullet}$	Lu_i	A_i	+3

formed to validate the predictions of the potential on select reactions. The DFT calculations were performed using the VASP code[24–26]. All calculations used the PBE generalized gradient approximation (GGA) functional[27] and the project augmented wave method (PAW)[28] with a $2\times2\times2$ k-point mesh and a 400 eV plane wave cutoff. All atoms were relaxed until the maximum force on any atoms was less than 0.03 eV/Å while the cell volumes and shapes were held constant.

3 Results

3.1 Cation interstitial

The initial defect structure of the simulation is represented in Fig. 1a. Again, the initial structure consists of a Lu_{Ti}+Ti_{Lu} antisite pair and a Ti interstitial, labeled Ti_i. This defect structure was chosen to represent a possible scenario that might occur in an irradiated material; the behavior of cation vacancies is discussed below. This defect configuration is not one that would be common or even critical in an irradiated environment, but provides a limiting case in which individual mechanisms and reactions can be identified, characterized, and understood. It thus is a model case to best understand the possible behavior of cation defects and their interaction with antisite defects.

The very first event in the course of the simulation is for the Ti interstitial to transform to a Lu interstitial and a Ti antisite (Lu_i+Ti_{Lu}). This process has a very large barrier with this potential (2.9 eV) and is significantly uphill in energy; the Lu_i+Ti_{Lu} structure is 1.9 eV higher in energy than the initial Ti_i structure. Even so, this is fastest process that can occur from this configuration. Events involving the direct motion of the Ti interstitial are possible, with a slightly higher barrier of 3.0 eV, though these were not accepted in the course of the simulation, presumably because the prefactor for these types of processes is lower. However, this highlights the delicate balance between rates that dictates the observed behavior, a point which will be discussed further below.

Once the Lu_i is formed, it then diffuses away from the Ti_{Lu} antisite, as both are positively charged: the interstitial has a net charge of +3 while the antisite has a net charge of +1. The electrostatic repulsion thus leads to the interstitial diffusing away from the antisite. Now that the Lu_i has been created and is free to diffuse through the system (the barrier for Lu_i migration in otherwise perfect pyrochlore is 1.1 eV with this potential, as determined from a separate simulation in which only a Lu_i was introduced into the simulation cell; in that simulation, the Lu_i remained as an intact species throughout the simulation), it can interact with the original antisite pair. In particular, it is attracted to the Lu_{Ti} antisite, as this antisite has a relative charge of -1. Figure 2 illustrates one mechanism by which the interstitial interacts with this antisite. First, the Lu_i pushes a matrix Ti ion off of its lattice site (not shown), effectively creating Lu_{Ti}+Ti_i. The Ti ion then pushes the original Lu_{Ti} into an interstitial position. The effective reaction is Lu_i+Lu_{Ti} → $(Lu_{Ti}+Ti_i)^*$ →Lu_{Ti}+Lu_i, where the starred complex is the transition state. The net effect is that the Lu_{Ti} antisite migrates against the interstitial and around the Ti_{Lu} antisite. Presumably, this is the same mechanism that would be responsible for Lu_{Ti} migration for isolated Lu_{Ti} antisites. The barrier for this process is 1.8 eV. The change in energy for this particular calculation is slightly endothermic; this is a consequence of the second Ti_{Lu} in the system (the distances between the various defects and the second Ti_{Lu} are different in the initial and final states).

A second type of event can occur via the interaction of the Lu_i and the Lu_{Ti}+Ti_{Lu} antisite pair, as illustrated in Fig. 3. In

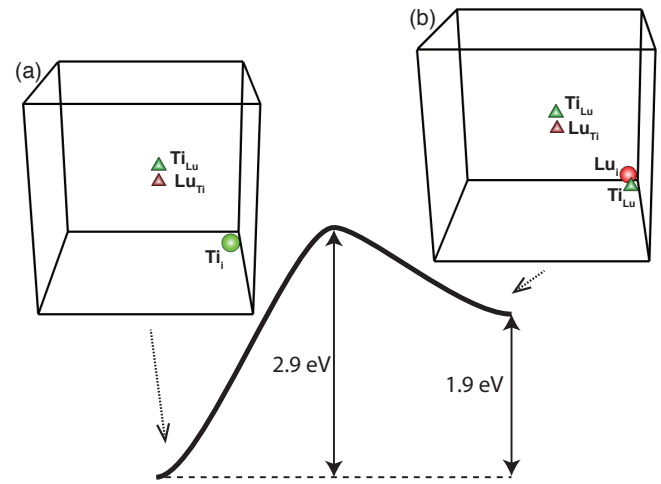

Fig. 1 The transformation of Ti_i →Lu_i+Ti_{Lu}. (a) Before the event and (b) after the event. The energy landscape associated with the event is schematically illustrated with the associated energies describing the process. Spheres represent interstitials and triangles antisite defects. Red indicates Lu defects while green represents Ti defects. Defects are identified by comparing to a perfect reference pyrochlore structure and using a 1 Å cutoff to identify ions that are not in the reference structure (interstitials) or vice versa (vacancies).

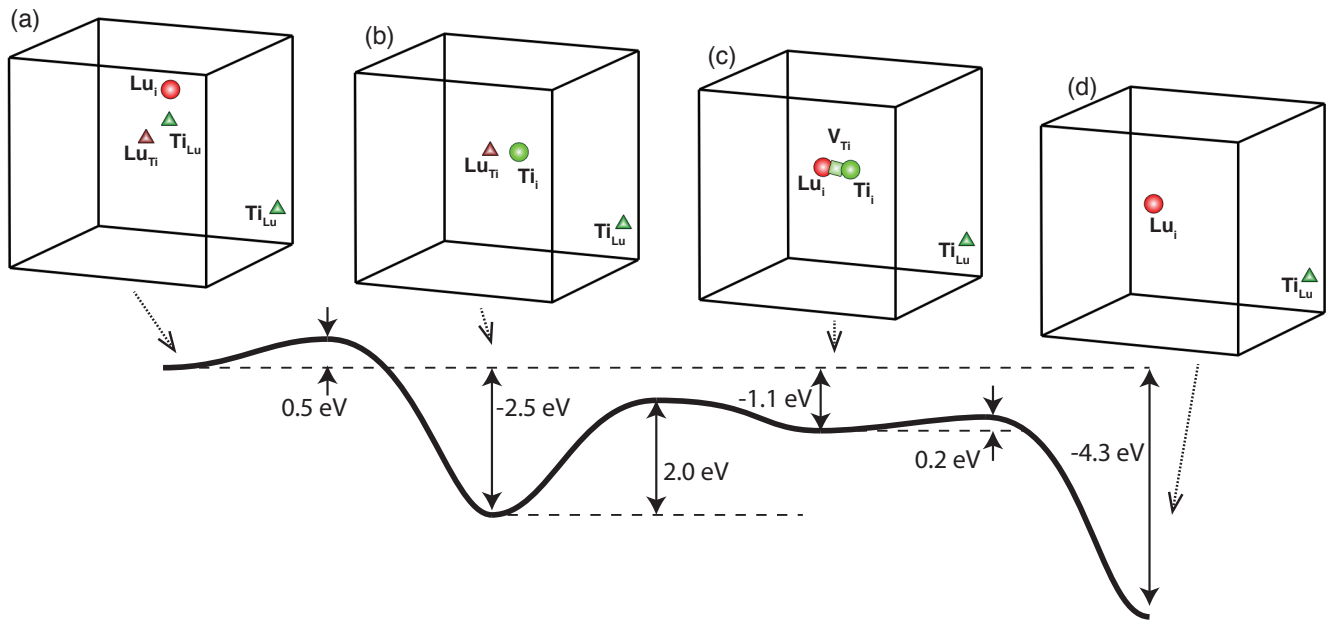

Fig. 3 The annihilation of Lu_{Ti}+Ti_{Lu} via a Lu interstitial. (a) Before the first event, Lu_i is nearest neighbor to the Ti_{Lu} component of the antisite pair. (b) Lu_i pushes the Ti ion in the antisite pair into an interstitial position, removing one half of the antisite pair. (c) The resulting Ti_i then pushes the remaining Lu_{Ti} off of its position, forming a split vacancy of mixed Ti and Lu character. (d) Completing the annihilation, Ti_i fills the resulting Ti vacancy, leaving behind only a Lu_i. The energy landscape associated with the event is schematically illustrated with the associated energies describing the process. Spheres represent interstitials, squares vacancies, and triangles antisite defects. Red indicates Lu defects while green represents Ti defects.

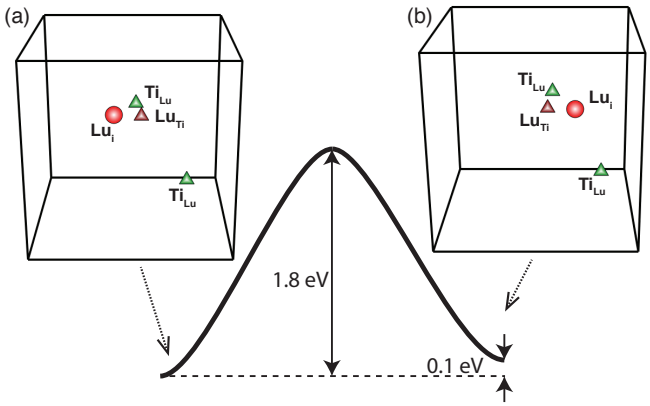

Fig. 2 The migration of Lu_i. (a) Before the event and (b) after the event. The energy landscape associated with the event is schematically illustrated with the associated energies describing the process. Spheres represent interstitials and triangles antisite defects. Red indicates Lu defects while green represents Ti defects.

this event, the Lu_i approaches the antisite pair from the Ti side (Fig. 3a). It first pushes the Ti_{Lu} into an interstitial position, creating a Ti interstitial (Fig. 3b): Lu_i+Ti_{Lu}+Lu_{Ti} →Ti_i+Lu_{Ti}. This reaction has a relatively small barrier of 0.5 eV, but is exothermic, lowering the energy of the system by 2.6 eV. Next, as shown in Fig. 3c, the Ti interstitial pushes the Lu antisite off of its position, creating a split vacancy structure in which both a Ti and Lu interstitial share a Ti lattice site within the pyrochlore structure (represented here as a vacancy). This process has a barrier of 2.0 eV, and increases the energy of the system slightly, by 1.5 eV. Finally, completing the process, the Ti interstitial moves to fill the vacancy site with a very small barrier of 0.2 eV, leaving behind a Lu interstitial. The reaction between Fig. 3b-d can be represented as Ti_i+Lu_{Ti} →Lu_i, with a complex intermediate state in which the split/mixed interstitial forms. Thus, the interaction of the Lu interstitial with the antisite pair leads to the annihilation of the pair. After the antisite pair has been annihilated, the total energy of the system has dropped by -4.4 eV, a consequence of the strong preference for ordering exhibited by the Ti pyrochlore[29].

After the annihilation event, the only defects remaining in the simulation cell are a Lu interstitial and a Ti antisite. Eventually, as Lu_i diffuses through the cell, these two defects interact. As illustrated in Fig. 4a, the interstitial can push the Ti out of its lattice site, momentarily removing the antisite from the system by

This journal is © The Royal Society of Chemistry [year]

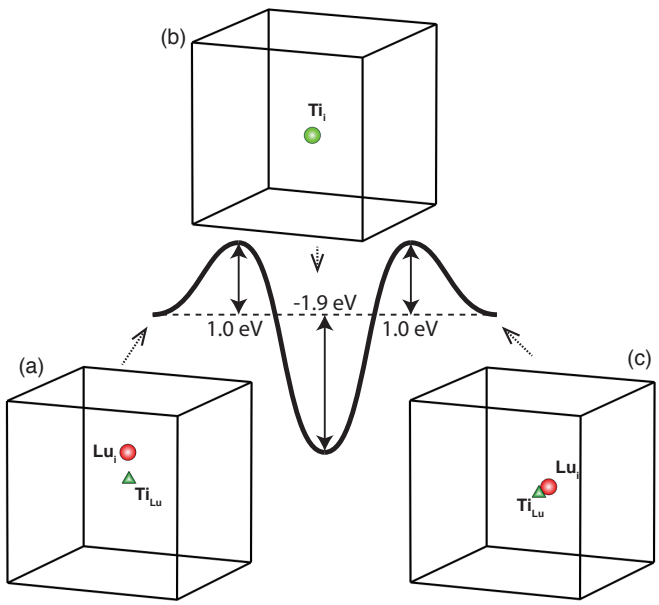

Fig. 4 The migration of Ti_{Lu}. (a) Lu_i+Ti_{Lu}. The Lu_i pushes out the Ti antisite, forming (b) Ti_i. This interstitial, in turn, pushes out a different Lu ion, recovering the Lu_i+Ti_{Lu} but with a net translation of Ti_{Lu}, as shown in (c). The energy landscape associated with the event is schematically illustrated with the associated energies describing the process. Spheres represent interstitials and triangles antisite defects. Red indicates Lu defects while green represents Ti defects.

creating the Ti_i that was present at the start of the simulation. This process, which is the reverse of the initial event shown in Fig. 1, has a barrier of 1.0 eV. Further, the energy of the Ti_i defect is 2.0 eV lower than the Lu_i+Ti_{Lu} defect, consistent with the energetics described in Fig. 1. However, just as in Fig. 1, the Ti_i cannot diffuse readily on its own, and the faster kinetic pathway is for it to again push out a Lu ion from its lattice site, recreating the Lu_i+Ti_{Lu} defect, shown in Fig. 4c. This process has a large barrier of 3.0 eV, the same as the process illustrated in Fig. 1. As there are multiple Lu neighboring the Ti_i that it can interact with, if the Lu ion that is ultimately pushed out is different than the one that came in as an interstitial in Fig. 4a, this net consequence of this interaction is the migration of the Ti_{Lu} antisite.

3.2 Cation vacancy

Under irradiation, both interstitials and vacancies are created. Further, under equilibrium conditions more appropriate for sintering conditions, vacancies will be present in much higher concentrations than interstitials. Thus, to provide insight into these conditions, we have also examined the behavior of a cation vacancy in $Lu_2Ti_2O_7$. The simulation began with a nearest neighbor antisite pair – as was done in the case of the interstitial simulations – and a Ti vacancy. As with the Ti interstitial, the first event leads to the transformation of the vacancy into a Lu antisite and a Lu vacancy, a reaction that has a barrier of 1.6 eV. Once created, the Lu vacancy can then migrate with a barrier of 3.4-4.0 eV (depending on the relationship to the other defects). However, the barrier for the Lu vacancy to interact with the antisite pair is very large and thus was not directly observed in the TAD simulations. Rather, we estimate the energetics of the reaction directly using the NEB method. The pathway is illustrated in Fig. 5. The first event in the process, in which the Lu vacancy annihilates the Lu antisite, creating a Ti vacancy, has a barrier of 4.8 eV, significantly higher than any barrier observed in the case of the interstitial. The resulting complex is relatively high in energy, 3.8 eV higher than the structure containing the Lu vacancy. With an additional barrier of 1.8 eV (5.6 eV relative to the original complex), the Ti vacancy can annihilate the Ti antisite, resulting in a lone Lu vacancy. The annihilation reaction liberates 4.1 eV as compared to the original Lu vacancy/antisite pair. Thus, the overall behavior of the cation vacancy is similar to that of the interstitial – the B cation vacancy is dynamically unstable, decaying to an A cation vacancy and A antisite, and the resulting A cation can heal antisite disorder – but the associated barriers are much higher (4-5.5 eV as compared to 0.5 eV for the interstitial).

3.3 Other pyrochlore chemistries

In order to determine the generality of the results obtainted on $Lu_2Ti_2O_7$, we performed shorter TAD simulations for a variety of A (La^{3+}, Sm^{3+}, Gd^{3+}, Tb^{3+}, Y^{3+}, Ho^{3+}, Yb^{3+}, Lu^{3+}) and B (Ti^{4+}, Mo^{4+}, Hf^{4+}) pyrochlore chemistries. Although not exhaustive, this selection of elements spans a large range of ionic radii – from 1.16 to 0.98 Å for the A cation, and 0.61 to 0.71 Å for the B cation – and ionic radii ratio r_A/r_B – 1.38 to 1.92. In addition, all but a few of the compounds represented by these chemistries have been observed with the pyrochlore structure. This is in contrast with, for instance, most Ce-based compounds ($A_2Ce_2O_7$), which were only observed as disordered fluorite, or Sc-based compounds, which form δ-$Sc_4B_3O_{12}$ rather than pyrochlore[30]. Zr, Sn, and Ru B cations, which also form stable pyrochlores, were excluded for diverse reasons: Zr, as was mentioned earlier, exhibits high oxygen mobility even in the ordered material[19] which significantly reduces the efficiency of the TAD algorithm; Ru is known to have multiple valence states, which can not be accounted for by the simple Buckingham form; Sn has a more covalent character than other B cations, which also prohibits the use of the Buckingham potential form for accurate results. That said, we have included the A cation Tb in our study. Tb can also adopt multiple valence states[31]. However, DFT studies have shown the disordering energetics of Tb-bearing pyrochlores to follow a linear relationship with ionic radius[29]. This suggests that $Tb_2B_2O_7$ pyrochlores are not departing from other A-chemistries and thus we expect the Tb^{3+} potential to accurately describe the

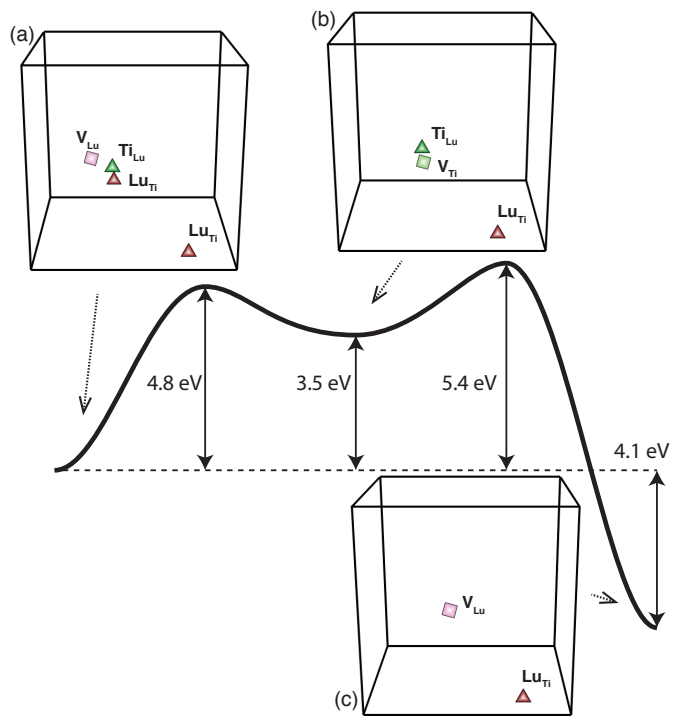

Fig. 5 The annihilation of Lu_{Ti}+Ti_{Lu} via a Lu vacancy (V_{Lu}). (a) V_{Lu} resides next to the Lu_{Ti}+Ti_{Lu} antisite pair. (b) The Lu_{Ti} antisite fills the V_{Lu}, leaving behind a V_{Ti} which can then (c) annihilate the Ti_{Lu} antisite. At the end of the process, only a lone V_{Lu} remains. The energy landscape associated with the event is schematically illustrated with the associated energies describing the process. Squares represent vacancies and triangles antisite defects. Red indicates Lu defects while green represents Ti defects.

disordering behavior in this compound. Finally, we have considered one chemistry, $La_2Ti_2O_7$ which does not, in reality, adopt the pyrochlore structure[32]. However, the potentials predict it to be at least metastable in the pyrochlore structure and it thus represents an extreme point in the compositional space to help identify trends.

One behavior found to be common to a majority of the chemistries considered is the decay of the initial B interstitial into an A interstitial and a B_A antisite, similar to the process described in Fig. 1. In these compounds, B_i is unable to diffuse independently as a species. However, for some chemistries, the B interstitial is the diffusing species. Either the decay $B_i \rightarrow B_A + A_i$ does not take place at all (in $La_2Ti_2O_7$, $Sm_2Ti_2O_7$, and $Gd_2Ti_2O_7$) or it does occur but then reverses and B_i diffuses ($La_2Mo_2O_7$, $Y_2Ti_2O_7$, and $Tb_2Ti_2O_7$). This diffusion often occurs through complex mechanisms, involving split interstitials, either as an intermediate state ($B_i \rightarrow (B_i + V_B + B_i) \rightarrow B_i$) or as the dominant structure of the diffusing interstitial [$(B_i + V_B + B_i) \rightarrow (B_i + V_B + B_i)$]. Once the B interstitial is in a split structure, it cannot directly decay to the $B_A + A_i$ structure. The typical barrier for split B_i migration, when it can occur, is much lower than for A_i migration ($\sim$ 0.6 ev, vs 1-1.2 eV), though the formation of a split interstitial complex involves high barriers. The barriers to transform from a pure B_i interstitial structure to a split ($B_i + V_B + B_i$) structure is about 2.8 eV. Thus, while split B_i interstitial migration can be fast, activating that fast migration mechanism will be slow. Exactly how these two processes combine to dictate the overall migration on the B sublattice needs to be further examined. Finally, no cation diffusion was observed in $Lu_2Hf_2O_7$. Much like in the B=Zr compounds, the oxygen ions diffuse quickly in the material, and these fast events prevent the observation of the slower cation migration events.

The case of $Gd_2Mo_2O_7$ is more complex. In this material, many decay and recombination events ($B_i \rightarrow B_A + A_i \rightarrow B_i$) were observed, occasionally punctuated by simple $B_i \rightarrow B_i$ migration. The back and forth between B_i and $B_A + A_i \rightarrow B_i$ can lead to net migration of the complex, though other behaviors are also observed. For example, at some point, after the $B_i \rightarrow B_A + A_i$ decay, A_i breaks away, much as in $Lu_2Ti_2O_7$. Just as in that case, A_i eventually makes its way to the antisite pair, annihilating only half of it, forming $B_i + A_B$. Once this happens, in contrast to what was described in Fig. 3, in $Gd_2Mo_2O_7$ the B_i diffuses away as a split interstitial. Thus, this compound exhibits a mix of behaviors in which either A_i or B_i migration can occur.

The migrating species – A_i or B_i – versus pyrochlore chemistry, as found from the TAD simulations, are summarized in Fig 6, along with the ionic radius ratio of the cations in the corresponding pyrochlore. It can be seen that the ionic radius ratio effectivily predicts which cation interstitial species, when starting with B_i, is the diffusing defect in pyrochlores: for $r_A/r_B < \sim 1.68$, the B_i decays into an antisite B_A and an interstitial A_i which diffuses; for

This journal is © The Royal Society of Chemistry [year]

$r_A/r_B > \sim 1.68$, B_i diffuses. That $Gd_2Mo_2O_7$ exhibited a mixed A/B migration character makes sense, then, as this compound resides at the border between the two behaviors ($r_A/r_B = 1.62$) and the system oscillates between the two behaviors.

One must keep in mind that these are kinetic processes, and, in particular, their relative rates depend on temperature. In fact, three mechanisms are competing here: the decay of B_i to A_i, the diffusion of B_i, and the diffusion of A_i. In order to predict which mechanism will dominate at a given temperature, one needs complete knowledge of the relative rates for each event, which will also depend on chemistry. This analysis is beyond the scope of this paper.

As mentioned, a few simulations on these other chemistries were evolved for longer times, allowing in some cases the observation of antisite migration (see Fig. 2) and antisite pair annihilation (Fig. 3) events in these other chemistries. For compounds in which the B interstitial is the migrating species, only one antisite comprising the antisite pair was ever annihilated, with the other remaining: $B_i + (A_B + B_A) \rightarrow A_i + B_A$. The two remaining defects both have a positive net charge (see Table 2), and this repulsion may be the reason that the second step of the annihilation reaction does not occur.

The comparison of cation interstitial behavior in different pyrochlore chemistries extends the insights obtained for $Lu_2Ti_2O_7$: the decay of B_i to A_i is common, though not universal, and the ionic radius ratio appears to dictate its probability; the annihilation of an antisite pair occurs via the migration of an A defect, but is limited in the case of a migrating B defect due to electrostatic repulsion between defects; migration on the cation sublattices occurs via complex mechanisms, invloving the formation of defect complexes and split interstitials.

3.4 Validation with density functional theory

Finally, to validate the results of the empirical potentials described above, DFT calculations were performed on selected reactions. Because of the system-size limitations of DFT, three reactions that could be treated in a smaller computational cell were considered: $Tu_i \rightarrow Lu_i + Ti_{Lu}$, the migration of Lu_i, and $Lu_i + V_{Lu} \rightarrow Lu_{Ti} + Ti_{Lu}$. The first two represent processes already discussed in this manuscript while the third, describing the recombination of an A cation Frenkel pair, was discussed in Ref.[7] and is included here for further validation of the potential. In these calculations, as opposed to the simulations described previously, there were no other defects in the simulation cell, because of the system size limitations of DFT. We note that the computational cells used in the DFT calculations, one unit cell of pyrochlore, are much smaller than those used in the potential simulations ($2 \times 2 \times 2$ unit cells) and thus the comparison between the two is less than optimal.

Table 3 compares results found with DFT and the Buckingham potential. In the case of the DFT calculations, two cases are considered: a fully neutral case and one in which the net charge of the computational cell is the same as that of the Buckingham potential simulations. Typically, there is better agreement between DFT and the potential for barriers than there is in the change in energy for the reaction. Further, there is little difference between the neutral and charged cases. Overall, however, the trends found with the potential agree with those determined with DFT, consistent with previous efforts to validate these types of potentials[34,35]. All calculations agree on whether each reaction is endothermic or exothermic. Barriers for the reactions agree to better than 1 eV. These calculations indicate that the behavior predicted with the potentials is not unphysical. However, they also highlight the fact that which mechanism dominates may be very sensitive to the details of the computation. For example, the DFT predicts that the initial decay reaction is easier than does the potential, but that the subsequent migration of Lu_i is slower. Thus, whether Lu_i, once formed, is able to break away may differ in the two sets of calculations. This likely means that the border between B_i and A_i dominated diffusion in Fig. 6 will still exist, but may shift to a different set of chemistries.

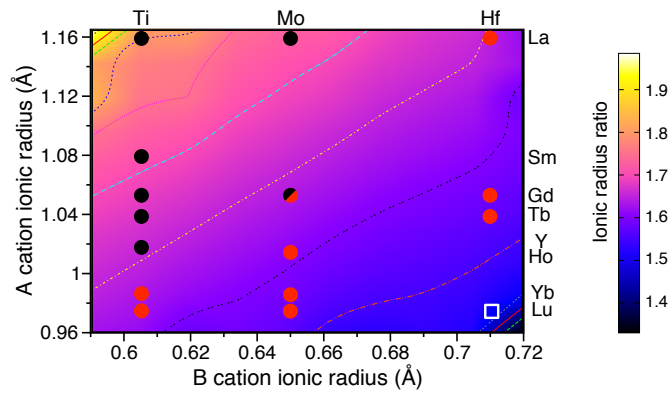

Fig. 6 Migrating cation species in $A_2B_2O_7 + B_i$ pyrochlores when starting with B_i. Black circles: B_i is the diffusing species; Red circles: A_i is the diffusing species, after the decay process $B_i \rightarrow B_A + A_i$ (see Fig. 1); Red and black circle: mixed migration character (see text). White hollow square: no cation diffusion was observed, due to limitations in the simulation methodology. The contour plot represents the ionic radius ratio r_A/r_B. All ionic radii are taken from Ref.[33]. The lines indicate contours of constant ionic radius ratio.

4 Discussion

The simulations described above reveal that cation dynamics in complex oxides such as pyrochlore can be rather involved. First, often, though not universally, B cations do not diffuse in isolation in pyrochlore. In such cases, they only diffuse when interacting with B defects. Williford and Weber also found that B vacancies can easily exchange with the A sublattice[36]. Second, defects created on the B sublattice are not always kinetically stable

Table 3 Energetics (changes in energy and saddle point energy) for select reactions as calculated with density functional theory (DFT) and the Buckingham potential. In the case of the DFT calculations, two charge states were considered (where appropriate).

Reaction	Change in energy (eV)			Saddle point energy (eV)		
	DFT neutral	DFT charged	Potential	DFT neutral	DFT charged	Potential
$Ti_i \rightarrow Lu_i + Ti_{Lu}$	1.1	1.0	1.9	1.3	2.0	3.0
Lu_i migration	–	–	–	2.1	2.0	1.1
$Lu_i + V_{Lu} \rightarrow Lu_{Ti} + Ti_{Lu}$	-4.1	n/a	-12.8	1.8	n/a	1.8

and can transform, again depending on the chemistry of the pyrochlore, into defects on the A sublattice and antisite complexes (e.g., $B_i \rightarrow A_i + B_A$). Even though this transformation can be uphill in energy, this is the fastest kinetic process in the system and the fastest pathway for migration of B cations.

Similar behavior has been observed in other complex oxides, notably AB_2O_4 spinels and ABO_3 perovskites.[9–11,37]. (We take the convention here that the B cation is the cation with the higher valence.) Just as B_i can decay to $A_i + B_A$ in pyrochlore, similar processes have been observed for Al in $MgAl_2O_4$ (Ref.[10]) or Ti in $SrTiO_3$ (Ref.[11]). Again, this behavior is not universal, as Ti interstitials in $BaTiO_3$ do not decay, but, rather like those pyrochlores with a large ionic radius ratio, migrates independently[11].

When the results here are combined with the insights gained on spinels and perovskites, a general trend emerges. In some complex oxides, cation diffusion does not occur independently on the two sublattices via defects intrinsic to each sublattice. Defects on the cation sublattice with the greater valence charge (Ti here, Al in the $MgAl_2O_4$ spinel, and Ti in $SrTiO_3$ perovskite) do not migrate through the material. Rather, they transform into defects on the other cation sublattice. Thus, in all three classes of complex oxides, there are examples where mass transport on the B sublattice is facilitated by defects on the A sublattice. Further, the creation of defects on the B sublattice naturally leads to cation antisite disorder in all three oxides. Given that the displacement threshold energy for displacing B cations under irradiation is higher than for A cations[38], one can imagine that, with the appropriate irradiation conditions, defects on the A sublattice could be preferentially created, leading to recovery of antisite disorder. At higher energies, however, B cations will also be displaced, creating a competition between the generation and recovery of antisite disorder.

However, as discussed above, while this behavior occurs for compounds in all three classes of complex oxides, it is certainly not universal and the details depend on the chemistry of the compound. Thus, predicting precisely in which compounds the cation behavior will be as complex as that predicted here in $Lu_2Ti_2O_7$ requires careful calculation of all of the relevant rates. Further, as multiple rates are indeed involved, the final behavior may very well be a function of temperature.

Finally, the oxygen sublattice also responds to these defects, but in a qualitatively different way. Compared to the defect-free pyrochlore structure, oxygen ions displace from their lattice sites when cation defects are present, but typically by only about half an angstrom. In none of the structures reported in Figures 1-5 did oxygen ions displace more than 1 angstrom. Thus, no oxygen ions moved from their lattice positions to fill the structural oxygen vacancies, or, equivalently, there was no rearrangement of the structural oxygen vacancy structure. The oxygen sublattice simply relaxed around the cation defects. We do note that the cation defects can only move in a subset of possible directions. For example, while both the A cation vacancy and interstitial are 12-fold and 6-fold coordinated by cations, respectively, migration only occurs in half of these directions, as that is where the A cations reside on the lattice. As the cation and oxygen vacancy structures are clearly correlated, these directions are equivalent in terms of local oxygen environment and thus we cannot specifically isolate the role of the oxygen structural vacancies in influencing the migration behavior of the cations.

In some of the simulations of the chemistries reported in Fig. 6, oxygen ions did displace by larger amounts (greater than 1 Å) into distinct local minima in the potential energy surface, though typically any such large displacement was transient and undone by the next event before any cations moved. However, these displaced oxygen can occasionally influence the migration paths of the cations. An example of this occuring in $Tb_2Hf_2O_7$ is provided in Fig. 7. The same cation event, the migration of the A cation interstitial, was observed twice during the course of the simulation, once as a pure hop of just the cation itself and once in the presence of displaced oxygen ions. The distorted oxygen structure became quite complex, as illustrated in the insets. Interestingly, in this particular case, the displaced oxygen ions actually hinder the migration of the A interstitial, effectively raising the barrier by about 1 eV. Thus, the interplay between the cation and anion sublattices can be extremely complex and can modify the potential energy landscape for the migrating cations. However, these larger oxygen distortions are not necessary for the movement of cation defects. Further, as has been noted by others[36], intrinsic oxygen vacancies, excess vacancies in addition to the structural vacancies, can form complexes with the cation defects that migrate faster than isolated cation defects. Here, we are interested in the unit mechanisms associated with cation defects, and we

This journal is © The Royal Society of Chemistry [year]

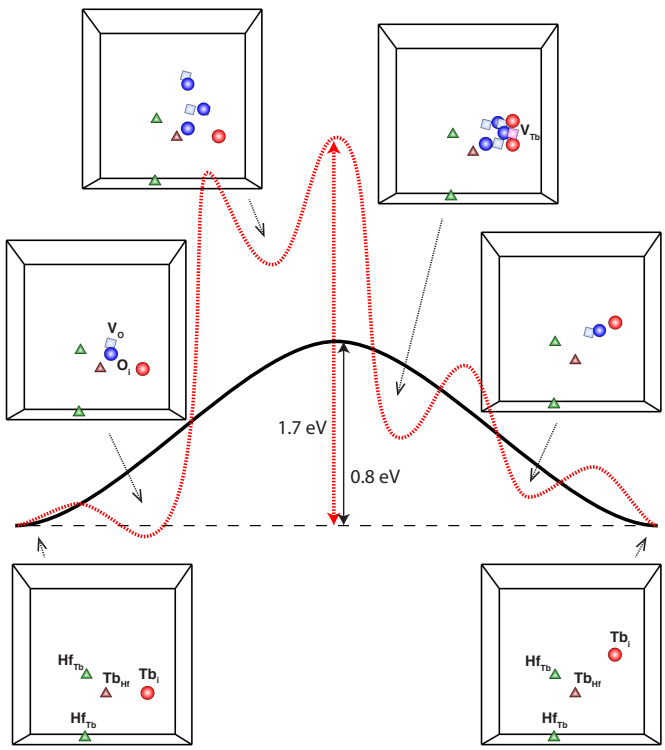

Fig. 7 Two pathways for the migration of an A cation interstitial in $Tb_2Hf_2O_7$ as identified from TAD simulations. For the path represented by the black solid curve, the cation interstitial makes a direct hop through one saddle point. For the path represented by the red dashed curve, the oxygen sublattice distorts around the cation defect structure into new local minima. This more complex pathway has a higher effective migration barrier.

have not considered the extra complexity that accompanies these more complicated defect structures.

In addition, more complicated processes can also occur – De Souza and Maier proposed a V_A+V_B di-vacancy mechanism coupling diffusion on both sublattices directly in perovskite[37]. We examined a similar mechanism in $Lu_2Ti_2O_7$ pyrochlore using TAD, illustrated in Fig. 8. The simulation shows that the Ti component of the di-vacancy again converts into a Lu vacancy and Lu antisite complex that is much lower in energy than the original structure. These simulations also show that eventually an oxygen interstitial is ejected from the complex, ultimately forming a $(2V_{Lu}V_{O}Lu_{Ti})$+O_i complex where the O_i is free to diffuse through the system with a barrier of roughly 2.5-3.0 eV. This example illustrates that more complex mechanisms can occur that do directly couple cation and anion kinetics, though they tend to occur for more complex defects such as the di-vacancy. When only one cation defect was present, we did not observe the subsequent formation of distinct oxygen defects.

5 Conclusions

To conclude, we used temperature accelerated dynamics (TAD) to simulate the kinetic processes associated with cation defects in pyrochlore. Taken with previous results on spinels and perovskites, these results highlight the rather complex behavior of cation defects that can occur in many complex oxides. Depending on the chemistry of the complex oxide, it is not sufficient to simply conceive of vacancies and interstitials on each sublattice. Rather, defect kinetics in these materials can be the result of a synergistic interaction between the two sublattices. Mass transport on one cation sublattice is directly related to the defect properties on the other sublattice and the diffusion of B cations, in particular, directly depends on the mobility of defects on the A cation sublattice. This is true for certain chemistries of pyrochlore, spinel, and perovskite, all of which have significantly different crystal structures, though the behavior is not universal in any of these oxides. Finally, whether this behavior occurs or not for a given chemistry depends on the relative ionic radii of the cations, suggesting that the dominant cation kinetic processes can be very different in different chemistries of the same crystal structure.

Acknowledgments

This work was supported by the U.S. Department of Energy, Office of Science, Basic Energy Sciences, Materials Sciences and Engineering Division. Los Alamos National Laboratory, an affirmative action equal opportunity employer, is operated by Los Alamos National Security, LLC, for the National Nuclear Security Administration of the U.S. DOE under contract DE-AC52-06NA25396.

References

1 S. Hull, *Rep. Prog. Phys.*, 2004, **67**, 1233–1314.
2 W. J. Weber, C. R. A. Catlow, L. W. Hobbs, H. Matzke, M. Nastasi and E. R. Vance, *J. Mater. Res.*, 1998, **13**, 1434.
3 D. Olander, *J. Nucl. Mater.*, 2009, **389**, 1.
4 R. H. E. van Doorn, H. J. M. Bouwmeester and A. J. Burggraaf, *Solid State Ionics*, 1998, **111**, 263–272.
5 M. Martin, *J. Chem. Thermodynamics*, 2003, **35**, 1291–1308.
6 A. Chartier, G. Catillon and J. P. Crocombette, *Phys. Rev. Lett.*, 2009, **102**, 155503.
7 Y. H. Li, B. P. Uberuaga, C. Jiang, S. Choudhury, J. A. Valdez, M. K. Patel, J. Won, Y.-Q. Wang, M. Tang, D. J. Safarik, D. D. Byler, K. J. McClellan, I. O. Usov, T. Hartmann, G. Baldinozzi and K. E. Sickafus, *Phys. Rev. Lett.*, 2012, **108**, 195504.
8 B. P. Uberuaga, D. A. Andersson and C. R. Stanek, *Current Opinion in Solid State and Materials Science*, 2013, **17**, 249–256.
9 B. P. Uberuaga, D. Bacorisen, R. Smith, J. A. Ball, R. W. Grimes, A. F. Voter and K. E. Sickafus, *Phys. Rev. B*, 2007, **75**, 104116.

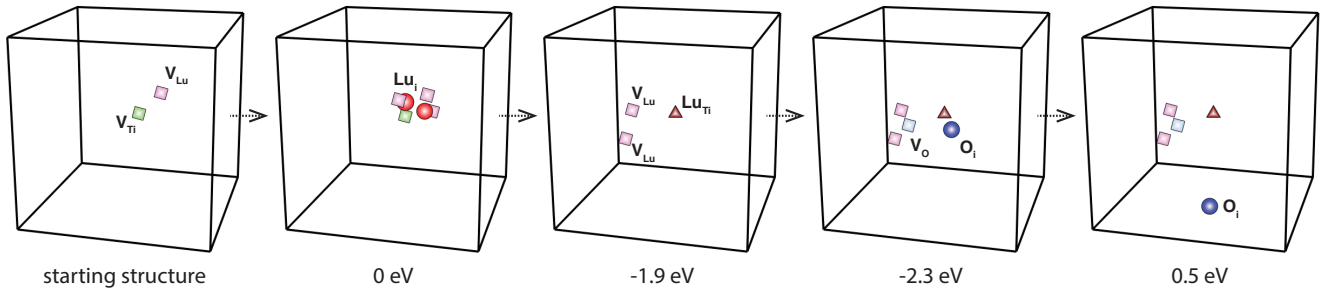

Fig. 8 TAD simulation of the evolution of a cation di-vacancy ($V_{Ti}+V_{Lu}$) in $Lu_2Ti_2O_7$. The initial structure is unstable and immediately reconstructs the local Lu sublattice. Eventually, the initial di-vacancy transforms into a complex involving two Lu vacancies and a Lu antisite. From this structure, an oxygen Frenkel pair nucleates (or, alternatively, an oxygen structural vacancy moves towards the two Lu vacancies). Ultimately, the resulting oxygen interstitial can diffuse through the lattice. The relative energies of the various structures are shown. The saddles are not shown in this case as there are many intermediate events that lead to these various structures.

10 S. T. Murphy, B. P. Uberuaga, J. B. Ball, A. R. Cleave, K. E. Sickafus, R. Smith and R. W. Grimes, *Solid State Ionics*, 2009, **180**, 1–8.

11 B. P. Uberuaga and L. J. Vernon, *Solid State Ionics*, 2013, **253**, 18–26.

12 T. Norby, *J. Mater. Chem.*, 2001, **11**, 11–18.

13 K. E. Sickafus, L. Minervini, R. W. Grimes, J. A. Valdez, M. Ishimaru, F. Li, K. J. McClellan and T. Hartmann, *Science*, 2000, **289**, 748–751.

14 K. E. Sickafus, R. W. Grimes, J. A. Valdez, A. Cleave, M. Tang, M. Ishimaru, S. M. Corish, C. R. Stanek and B. P. Uberuaga, *Nature Materials*, 2007, **6**, 217–223.

15 M. Sorensen, Y. Mishin and A. Voter, *Physical Review B*, 2000, **62**, 3658–3673.

16 D. Perez, B. P. Uberuaga, Y. Shim, J. G. Amar and A. F. Voter, *Annual Reports in Computational Chemistry*, 2009, **5**, 79.

17 R. A. Buckingham, *Proceedings of the Royal Society of London. Series A, Mathematical and Physical Sciences*, 1938, **168**, 264.

18 L. Minervini, R. W. Grimes and K. E. Sickafus, *J. Am. Ceram. Soc.*, 2000, **83**, 1873–1878.

19 R. Perriot and B. P. Uberuaga, *J. Mater. Chem. A*, 2015, **3**, 11554.

20 G. Henkelman, B. P. Uberuaga and H. Jónsson, *J. Chem. Phys.*, 2000, **113**, 9901.

21 F. A. Kröger and H. J. Vink, *Solid State Physics - Advances in Research and Applications*, Academic Press, New York, 1957.

22 C. Scott, R. Smith, B. P. Uberuaga and K. E. Sickafus, *Nuclear Instruments and Methods in Physics Research Section B: Beam Interactions with Materials and Atoms*, 2010, **268**, 3066–3070.

23 D. J. Bink, *Computer modeling of zinc oxides and related oxide ceramics*, Dept of Chemistry, University of Surrey, 1994.

24 G. Kresse and J. Hafner, *Phys. Rev. B*, 1993, **48**, 13115.

25 G. Kresse and J. Furthmuller, *Comput. Mater. Sci.*, 1996, **6**, 15.

26 G. Kresse and J. Furthmuller, *Phys. Rev. B*, 1996, **54**, 11169.

27 P. E. Blöchl, *Phys. Rev. B*, 1994, **50**, 17953.

28 G. Kresse and D. Joubert, *Phys. Rev. B*, 1999, **59**, 1758.

29 C. Jiang, C. R. Stanek, K. E. Sickafus and B. P. Uberuaga, *Phys. Rev. B*, 2009, **79**, 104203.

30 C. R. Stanek, C. Jiang, B. P. Uberuaga, K. E. Sickafus, A. R. Cleave and R. W. Grimes, *Physical Review B*, 2009, **80**, 174101.

31 M. P. V. Dijk, K. J. D. Vries and A. J. Burggraaf, *Solid State Ionics*, 1985, **16**, 211.

32 P. Gasperin, *Acta Cryst.*, 1975, **B31**, 2129.

33 R. D. Shannon, *Acta Cryst. A*, 1976, **32**, 751.

34 B. P. Uberuaga, R. Smith, A. R. Cleave, F. Montalenti, G. Henkelman, R. W. Grimes, A. F. Voter and K. E. Sickafus, *Physical Review Letters*, 2004, **92**, 115505.

35 B. P. Uberuaga, S. Choudhury, X.-M. Bai and N. A. Benedek, *Scripta Mater.*, 2012, **66**, 105–108.

36 R. E. Williford and W. J. Weber, *J. Am Ceram. Soc.*, 1999, **82**, 3266–68.

37 R. A. D. Souza and J. Maier, *Phys. Chem. Chem. Phys.*, 2003, **5**, 740–748.

38 R. Devanathan and W. J. Weber, *J. Appl. Phys.*, 2005, **98**, 086110.

This journal is © The Royal Society of Chemistry [year]